Measurement of Dynamic Properties of Vertical Gas-Liquid Flow

A. Hunt*, L.A. Abdulkareem† and B.J. Azzopardi†

* Atout Process Limited, 26-28 West Street, Bridport, Dorset DT6 3QP, United Kingdom

† Process and Environmental Engineering Division, Faculty of Engineering, University of Nottingham, UK

ahunt@atoutprocess.com

Keywords: Electrical Capacitance Tomography, gas-liquid flow, huge wave, churn flow, Wire Mesh Sensor

Abstract

Measurements of void fraction profiles, bubble sizes and velocity distributions are required to model two-phase flows and to understand their flow regimes and physics. This paper reports on the use of electrical capacitance tomography (ECT) to measure flow characteristics in gas-liquid flows in a vertical pipe. We report measurements over a range of liquid superficial velocities from 0.05 ms^{-1} to 0.5 ms^{-1} and gas superficial velocities from 0.06 ms^{-1} to 6 ms^{-1} in a pipe 6 m long of internal diameter 0.067 m.

A second complementary technique, a wire-mesh sensor (WMS), was also present in the tests and the results of the two sensors are shown to be within 2% of measurement on cross-sectional average void fraction. A previous paper using the same techniques (Azzopardi et al 2009) focused on the comparison of measurements of void fraction and bubble size between these two sensors. Here we pursue the mean values in terms of the drift flux model and potential applications of ECT as a flowmeter. We go on to use the velocity measurement capability of ECT to describe the velocity profiles in the flow and we show detailed measurements of void fraction profiles, wave and slug structures.

ECT has relatively low spatial resolution in comparison to the WMS, and as shown by reference to other measurements. It is however a high speed measurement (up to 5000 frames of data per second), gives velocity information and is completely non-intrusive and suitable for use in industrial pipelines. ECT requires good physical models of the relationship of void fraction to permittivity and we publish here a general equation for that relationship allowing for the shape of the voids. Our results demonstrate that ECT measures flow structure velocity rather than gas velocity, where those structures are typically small bubbles, large 'churn' bubbles', or 'huge waves' as described by Sekoguchi and Mori (1997). Given the capabilities of ECT to measure velocity non-intrusively we are able to show detailed void fraction and velocity profile information for these flows.

We observe three types of flow in these experiments: dispersed bubble, plug and huge wave. In dispersed bubble flows at higher liquid velocities and low gas flowrate the velocity profile exhibits a centre-peak, while for plug flows we a see flat velocity profile. An important transition is seen at a gas superficial velocity of about 1 ms^{-1} as huge waves become the dominant feature with a significant centre peak to the velocity profile. At this transition the velocity of the wave structure is about 2ms^{-1} and the transition is clearly measurable by the frequency of flow structures. Below the transition (in plug flow) the frequency increases with gas superficial velocity while above the transition (with huge waves dominant) the frequency is approximately constant. We believe that this transition point is associated with the moment at which gas from one plug structure 'breaks through' the liquid barrier to the higher one and a continuous gas core starts to exist in the flow.

Introduction

This paper reports on the use of two complementary techniques for making measurements of flow parameters in two-phase gas-liquid flow: electrical capacitance tomography (ECT) and a wire-mesh sensor (WMS). Both sensors were mounted on the same pipe and concurrent measurements were made over a period of 1 minute at each flow condition.

Comparisons between measurements using various combinations of imaging and other sensors in two-phase flows have been made in the past including: ECT and gamma-ray densitometers (Hunt, Pendleton and Ladam 2004); WMS and ECT (Azzopardi et al 2009); WMS and x-ray tomography (Prasser et al 2005); ECT and weigh scales (Hunt, Pendleton and Byars 2004). These comparisons have shown that for measuring dynamic properties of local flow ECT is fast, accurate, non-intrusive but with low spatial-resolution; while WMS is fast, accurate, of high spatial resolution but intrusive and disruptive of the flow.

In this paper we focus on the use of ECT to give detailed information about gas-liquid flows while using WMS as a check on the void measurement accuracy in this application.

Nomenclature

c	Constant in drift flux model
D	Pipe internal diameter
g	Acceleration due to gravity
n	Shape factor in permittivity equation
U	Velocity
v	Void fraction or concentration of dispersed phase

Greek letters

ε	Electrical permittivity

Subsripts

1	Continuous phase (in electrical equations)
2	Discontinuous phase (in electrical equations)
g	Gas
L	Liquid
m	Mixture
s	Superficial (flowrate divided by pipe area)

Electrical Capacitance Tomography

Electrical capacitance tomography (ECT) is a non-intrusive technique which can be used for imaging and velocity measurement in flows of mixtures of 2 non-conducting materials. Developments over the last 15 years have made fast, accurate measurement systems available for laboratory research. Using ECT can offer measurements unobtainable with other measurement technologies, but the interpretation of quantitative flow data requires a good physical model of the interaction of the materials with the electric field in the sensor and appropriate reconstruction and analysis algorithms. Hunt, Pendleton and Ladam (2004) reported suitable algorithms for flows of dry solids in air, here we study the requirements and results in gas-liquid flows.

An array of electrodes was arranged around the outside of the non-conducting pipe wall (see Figure 1) and all unique capacitance pairs were measured using a Tomoflow R5000 flow imaging and analysis system. The instrument contains 16 identical measurement channels and 16 identical driven guard circuits and in the tests reported here was operated with a twin-plane sensor.

Data can be captured at rates up to 5000 image frames per second with typical measurement noise level at 500 fps of 0.02fF rms. The typical average value between two opposite electrodes is 10fF. In the experiments reported here the frame rate was 1000 fps.

Measurements were made between all pairs of electrodes within each plane around the sensor using a charge/discharge capacitance technique. An excitation signal was used in the form of a 15V peak to peak square wave with a frequency of 5 MHz.

The sensor included a full set of driven guard electrodes running axially before, between and after the measurement planes giving a total of 5 axial sets of 8 azimuthal electrodes ensuring that an axially-uniform electric field was maintained over the capacitance sensor cross-section and the two sensor 'planes' (actually short cylindrical sections).

Inversion of the 28 capacitance pairs to a 812 pixel image on a 32x32 square grid was undertaken as described below, and component information (void fraction etc.) was extracted from these images.

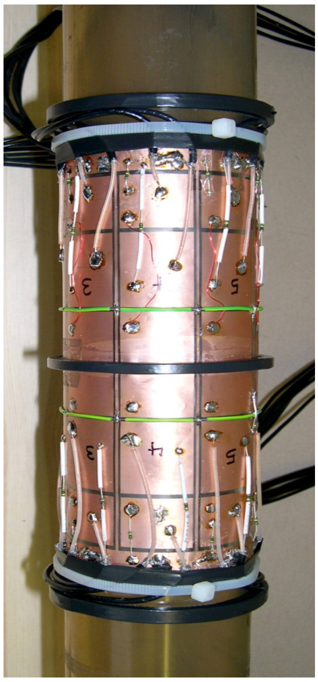

Figure 1: ECT sensor mounted on transparent plastic pipe with electrical guard removed for clarity.

Cross-correlation between the image planes gives the velocity distribution across the flow. The resolution of ECT images is limited (see example in Figure 2), so cross-correlation is not carried out for all pixels, but for a set of larger 'zones' containing the average of a number of pixels.

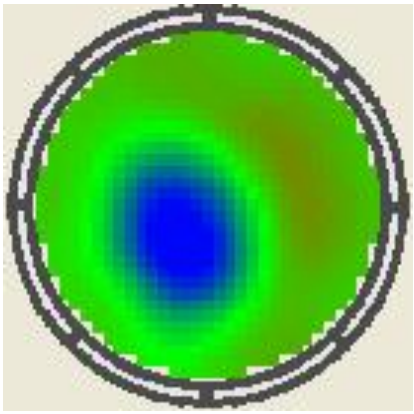

Figure 2: Typical 812 pixel image from ECT. A false colour scale runs from red (100% liquid) to blue (100% gas).

Most ECT sensors are non-linear, both in the relationship between the measured capacitances and the permittivity of the sensor contents and also in the relationship between the concentration of a 2-phase mixture and its effective permittivity. All images shown and used in this work were reconstructed using linear back-projection and a Tikhonov regularisation factor of 10, see Byars (2001) for more details of this technique.

Figure 2 shows a typical image from ECT with the cross-section of a large bubble in the lower left part of the pipe, with mostly liquid in the upper right. The intermediate permittivity (shown as green) indicates that the liquid has significant amounts of gas bubbles distributed in it that are below the resolution of the simple linear back projection reconstruction.

Experimental Facility

The experiments were carried out near the top of a 6m long pipe of internal diameter 0.067m. The pipe is mounted on a frame that can be inclined at any angle from from vertical to 20° above horizontal, though the tests reported here were only measured in vertical flows. Figure 3 shows a photograph of the test rig in vertical position.

Figure 3: Overall view of flow rig, the pipe test section is mounted on the yellow frame.

Silicone oil of density 910 kg.m^{-3} and viscosity 5 cSt was circulated through the pipe by a pump at a range of flowrates, while air was injected at the lowest part of the pipe before being vented off after leaving the test section.

Given the development length/pipe diameter ratio of approximately 75 it is believed that the gas distribution and bubble size at the working section were unaffected by the injection method.

The ECT sensor was mounted approximately 1m from the upper end of the test pipe with the WSM about 0.5m above it. It was not possible to mount the WSM below the ECT sensor as visual observation showed that the intrusive wire mesh of the WSM changed the nature of the flow completely by breaking up large bubbles and generally homogenising the flow.

Wire Mesh Sensor

In a wire-mesh sensor electrodes are stretched across the flow cross-section within two axially-separated planes. A fast electronic measurement system connected to the wires measures the relative permittivity ε at each crossing point. Scanning a complete cross-section of the flow can be done at up to 10 000 frames per second. The sensor employed in our experiments has 2 × 24 wires which have 2.8 mm separation and is the same as described by Azzopardi et al (2009).

Estimation of void fraction from permittivity

For the WMS the choice of permittivity model is not critical as the gap between the wires is small and is essentilly either filled with liquid or with gas.

For ECT however, the choice of physical model is critical. The capacitance measurement in ECT is converted to electrical permittivity using a look-up table linearisation from calibration at various permittivities. To move from this electrical measurement to a fluid-mechanically useful measure of concentration or void fraction (terms used here interchangeably) involves the use of a physical model linking the two. The expression used by Hunt, Pendleton and Byars (2004) as the 'Maxwell' model applies to non-conducting spheres distributed uniformly in a non-conducting medium.

$$\varepsilon_m = \varepsilon_1 \,[1 + 3.v.(\varepsilon_2 - \varepsilon_1)/(\varepsilon_2 + 2.\varepsilon_1 - v.(\varepsilon_2 - \varepsilon_1))] \qquad (1)$$

where ε_m is the effective mixture permittivity of a distribution of spherical particles, ε_1 is the material permittivity of the continuous medium, ε_2 is the material permittivity of the spherical particles, and v is the volumetric fraction of space occupied by the spheres.

For comparison purposes we will also refer to simple models where the measurement represents simple arrangements of material between the plates of a parallel capacitor. These simple systems are effectively the upper and lower bounds for all permittivity-concentration models

The 'parallel' model applies when the dielectric material is distributed as parallel plates normal to the capacitor plates:

$$\varepsilon_m = \varepsilon_1.(1-v) + \varepsilon_2.v \qquad (2)$$

and the 'series' model is the model for capacitances in series when the dielectric material is distributed as plates parallel to the electrodes:

$$\varepsilon_m = (\varepsilon_1 . \varepsilon_2)/ (\varepsilon_1 . v + \varepsilon_2.(1 - v)) \quad (3)$$

See PTL Application Note 4 (1999) for a more complete description of these simple expressions.

Wagner (1914) gave the original derivation of the electric field through an array of distributed spheres, based on equations proposed by Maxwell in 1873. Van Beek (1960) quotes from Sillars (1937) giving a more general form of Wagner's derivation:

$$\varepsilon_m = \varepsilon_1 [1 + n.v.(\varepsilon_2 - \varepsilon_1)/(\varepsilon_2 + (n\text{-}1). \varepsilon_1)] \quad (4)$$

where n is a function of particle shape. For spheres $n = 3$ and then equation 4 reduces to equation 1. For oblate spheroids n ~ 1 and for prolate spheroids $n > 3$. We refer to equation 4 as the Maxwell-Wagner-Sillars (MWS) equation.

Hunt (2007) introduced the same factor n into equation 1 by analogy to derive a more generalised form:

$$\varepsilon_m = \varepsilon_1 [1 + n.v.(\varepsilon_2 - \varepsilon_1)/(\varepsilon_2 + (n\text{ -}1). \varepsilon_1 - v.(\varepsilon_2 - \varepsilon_1)] \quad (5)$$

This extended expression is we believe novel and has the significant advantage that it allows for the particles to be non-spherical and reduces to the other forms as follows:

$n = 1$: series model
$n = 3$: Maxwell-Rayleigh
$n = \infty$: parallel model.

Previous experiments with gas-liquid flows led us to choose n=100 for the results presented here, this choice being justified by the comparisons shown in the next section.

Cross-sectional average values

The mean void fraction was calculated from each sensor using the average of all ECT pixel values and the average of all WMS nodes over the 60 seconds of data taken at each flow condition. Figure 4 shows these results plotted against each other.

It can be seen from Figure 4 that the two sensors agree on average void fraction to within 2% of reading for most of the flows measured. The liquid superficial velocity varies from 0.05 ms^{-1} to 0.524 ms^{-1} and the gas superficial velocity from 0.06 ms^{-1} to 6.05 ms^{-1}.

The flows measured in this set of experiments visually exhibited three basic patterns: bubbly flows, through plug to huge wave structures. The terminology and flow pattern conditions are consistent with those described in Sekoguchi et al (1997) who first described the 'huge waves'.

The cross-correlation process used in ECT estimation of velocity emphasizes the largest scale changes in concentration, which are associated with the passage of gas bubbles, clusters of bubbles, slugs, churn structures or liquid waves and films, as the gas velocity increases.

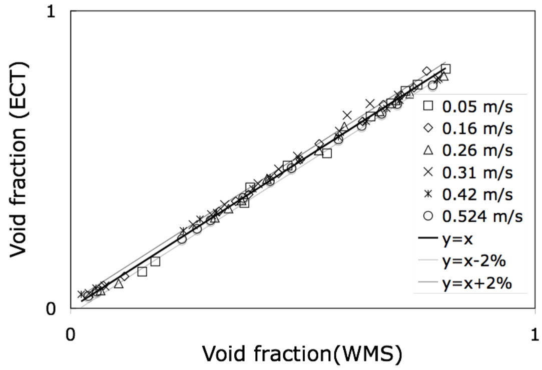

Figure 4: Average void fraction from each sensor. Velocity figures for each data set refer to different liquid superficial velocities.

Velocity measurements were taken from the twin-plane ECT system by cross-correlating the concentration time signal in the same zone of the two axially-separated measurement planes. For this purpose each plane was divided into 13 roughly equally-sized zones as in described by Hunt, Pendleton and Ladam (2004). The resulting velocities were averaged to give the 'average ECT velocity', while the void-fraction-weighted average of the velocities is equivalent to a calculation of superficial velocity.

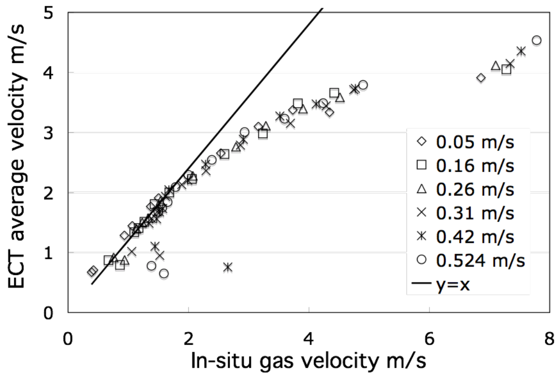

Figure 5: Average ECT velocity plotted against in-situ gas velocity calculated from reference gas flowrate and void fraction measured by WMS. Velocity figures for each data set refer to different liquid superficial velocities.

The in-situ gas velocity, Ug, is related to the superficial velocity U_{gs} in the normal manner:

$$U_g = U_{gs} / v \quad (6)$$

where v is the void fraction. Figure 5 shows that for gas in-situ velocities below about 2 ms^{-1} the average ECT velocity represents the in-situ gas velocity, while at higher flowrates the average ECT velocity becomes less and less dependent on gas velocity.

These results suggest that below 2 ms^{-1} in-situ gas velocity the flow is dominated by dispersed gas bubbles so that the cross-correlation velocity is equal to the average gas velocity, at the highest gas flowrates the ECT average velocity represents the speed of passage of complex liquid structures moving slower than the gas.

Figure 6 shows the void-fraction weighted ECT average velocity plotted against the input gas superficial velocity. In conventional flowmetering this would be equivalent to a calibration curve of estimated flowrate against reference flowrate.

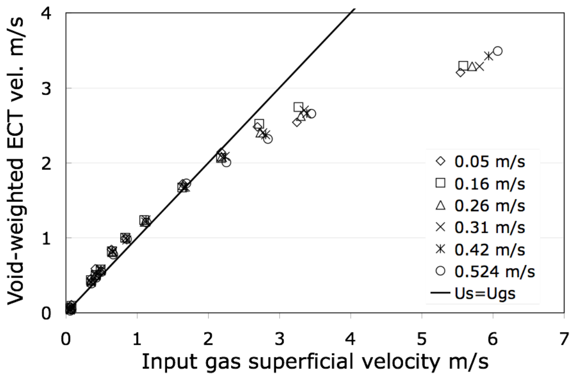

Figure 6: Average void-weighted ECT velocity plotted against reference superficial gas velocity. Velocity figures for each data set refer to different liquid superficial velocities.

It can be see from the figure that at low gas flowrates the average void-weighted ECT velocity tends to overestimate the gas superficial velocity, but above a value of about 2.5 ms^{-1} the difference becomes negative and of growing magnitude.

Use of ECT as a flowmeter in these conditions would require a calibration curve fitted to the graph in Figure 6. The effect of varying liquid superficial velocity appear to be small, but how general this would be is impossible to say.

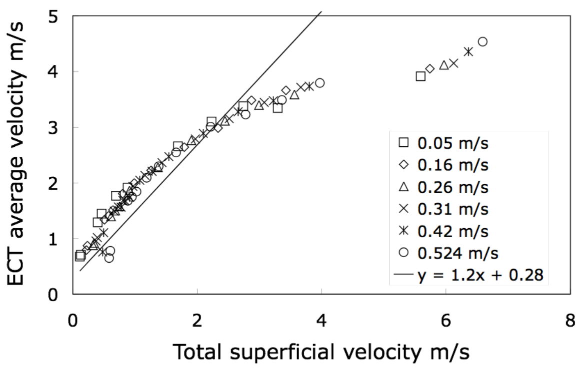

Figure 7: Average void-weighted ECT velocity plotted against reference superficial gas velocity. Velocity figures for each data set refer to different liquid superficial velocities.

We now compare our results to the drift-flux modelling approach. Nicklin et al (1962) first generalised the modelling of the rise velocity of single Taylor bubbles in the form:

$$U_g = c.(U_{gs} + U_{Ls}) + 0.35\,(g.D)^{0.5} \qquad (8)$$

where c took a value between 0.9 and 1.85 depending on the liquid velocity, but above a liquid velocity of 0.3 m/s took the value 1.2.

Figure 7 shows that while the slope of this line looks reasonable, the intercept should be much higher to fit the data in the range 0 to 1 ms^{-1} where we know from Figure 4 that the ECT average velocity is representative of the in-situ gas velocity.

We explain this discrepancy by remarking that the Nicklin model was established for smooth-fronted Taylor bubbles in a 25.4 mm diameter pipe, where the limiting factor to velocity is the passage of the liquid in the annular film around the bubble and the centreline velocity of the liquid in between the bubbles. In our work in a pipe of over 3 times the cross sectional area we observe that the irregular 'churn' bubbles seem visually to 'tunnel' up the pipe in the fast-moving wake of the preceding one. This, associated with the larger flow area available around the bubble for liquid backflow could explain such a difference. We return to this observation of 'tunnelling' below.

Void fraction profiles

One advantage of tomographic measurements is that measurements at particular points of interest can be defined after the measurement has taken place simply by defining the image zone of interest. To study the profile of void fraction across the pipe, a set of zones was defined as shown in Figure 8.

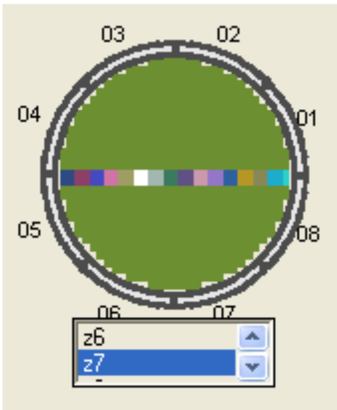

Figure 8: Zone map for void and velocity profiles. 16 zones of 2x2 pixels distributed equally along the horizontal diameter. Zone 7 highlighted in white, other colours are simply to distinguish the zones.

Taking the average of the 60 seconds of data for each set of experimental conditions for each zone enables to calculate the void fraction profiles across the flow. Examples are shown in Figures 9 and 10 for liquid superficial velocity of 0.06 ms^{-1} and 0.524 ms^{-1} respectively.

We can see from these figures that the void fraction profile is peaked at the centre of the pipe for all of the flows measured. As the gas flowrate increases at a given liquid flowrate the void fraction increases fairly uniformly until at high gas rates the centre of the pipe is almost completely empty of liquid.

For a given gas flowrate an increase in liquid flowrate gives a lower void fraction level so that the point at which the centre becomes gas-only is at a higher rate.

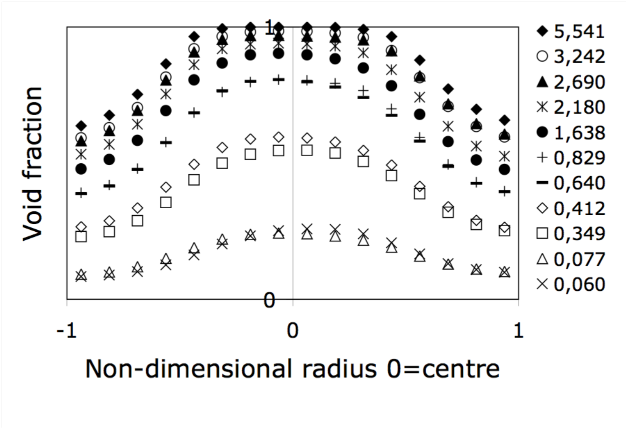

Figure 9: Void fraction profiles from ECT using zones as shown in Figure 8 at a liquid superficial velocity of 0.052 ms^{-1}. Numbers in the legend are gas superficial velocity in ms^{-1}.

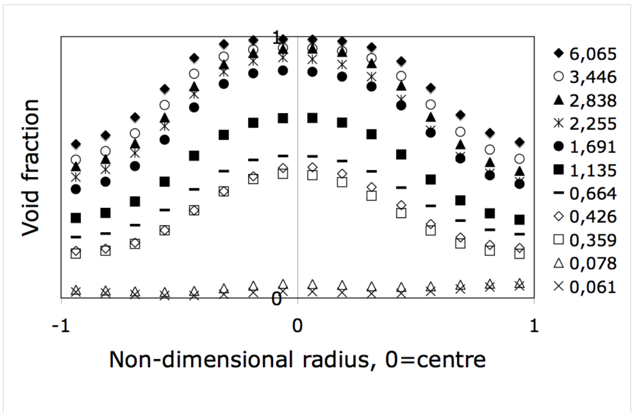

Figure 10: Void fraction profiles from ECT using zones as shown in Figure 8 at a liquid superficial velocity of 0.524 ms^{-1}. Numbers in the legend are gas superficial velocity in ms^{-1}.

Void fraction profiles can also be extracted from the WMS data and a comparison is shown between these and the ECT profiles in Figure 11. To eliminate some of the extraneous non-symmetric features from the profiles, Figure 11 shows half-pipe profiles where the two sides of the profile have been averaged.

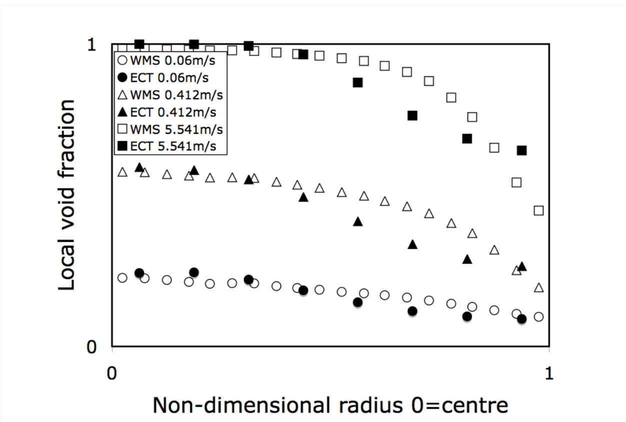

Figure 11: Void fraction profiles from ECT and WMS at a liquid superficial velocity of 0.052 ms^{-1}. Numbers in the legend are gas superficial velocity in ms^{-1}.

It can be seen from Figure 11 that the overall values of void fraction are similar (as shown also by the mean data in Figure 4) but that there are differences in form - the ECT data shows a consistent tendency to a shallow horizontal 'S' shape while the WMS data shows a steady decline towards the wall.

Previously published data from similar flows has shown profiles with simple central peaks rather as the WMS data (eg Couet *et al* 1990) and also profiles with wall peaking (eg Prasser *et al* 2005) so both forms shown here are possible within the range expected. While ECT can exhibit artefacts in reconstruction which might distort the profiles, WMS undoubtedly breaks up the bubble structure in the flow and so may distort the distribution. Further work is required to establish the cause of the differences shown here.

Velocity profiles using ECT

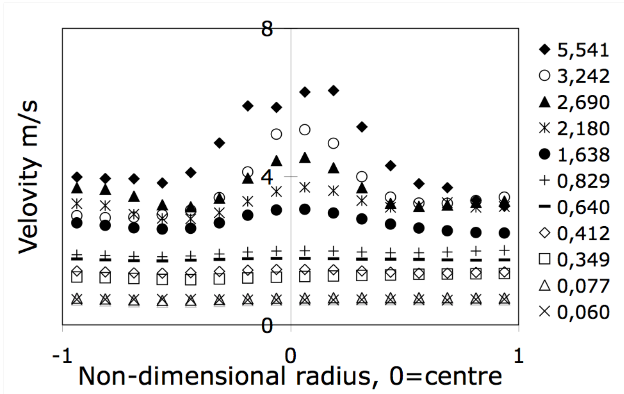

Figure 12: Velocity profiles from ECT using zones as shown in Figure 8 at a liquid superficial velocity of 0.052 ms^{-1}. Numbers in the legend are gas superficial velocity in ms^{-1}.

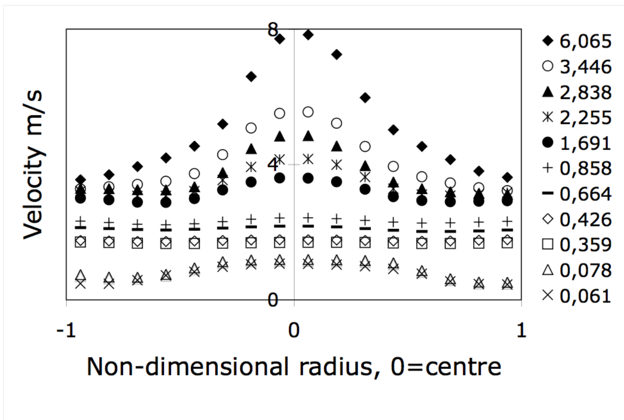

Figure 13: Velocity profiles from ECT using zones as shown in Figure 8 at a liquid superficial velocity of 0.524 ms^{-1}. Numbers in the legend are gas superficial velocity in ms^{-1}.

Whereas both ECT and WMS can measure the void fraction profiles, of the two only ECT can measure velocity. Using the same zone map as shown in Figure 8, we have calculated the transit velocity between the two ECT measurement planes by cross-correlating the time-varying concentration in each zone with the same zone in the second plane. Typical results are shown in Figures 12 and 13 for the same conditions as Figures 9 and 10.

Considering these velocity profiles we can see that, unlike the void profiles which all exhibited essentially the same form, there are three distinct types present. For high liquid flowrate and low gas flowrate the velocity profiles show centre peaks, for moderate gas rates at all liquid flowrates the profiles are flat, while at high gas flowrates for all liquid flowrates the velocity profiles are centre-peaked.

The transition between flat velocity profiles and centre-peaked is striking and occurs always at a gas superficial velocity of about 1 ms-1, the same value as that at which the ECT-measured flow structure velocity starts to deviate from the in-situ gas velocity (see Figure 5).

Measurement of flow structures using ECT

To consider the flow structures further we undertook simple power-spectral analysis of the ECT concentration time-series data, taking the value of the low-frequency peak as a measure of structure frequency of passage. Visual analysis of the time-series (as shown in Figure 16 and 17) confirms this frequency as being typical.

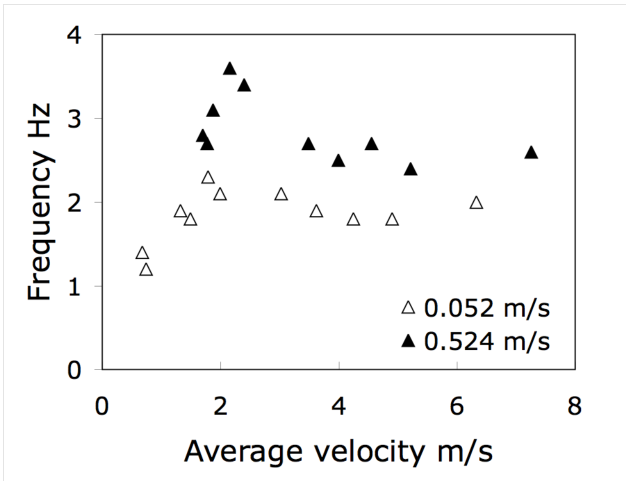

Figure 14: Structure frequency against velocity at non-dimensional radius of 0.1875 (zone 7). Numbers in the legend are gas superficial velocity in ms^{-1}.

From Figure 14 it can be seen that below an average velocity (that is the average ECT velocity zone 7) of about 2 ms^{-1} the passing frequency increases with velocity, while above point the frequency remains fairly constant, though lower than at the transition.

Dividing the average velocity by the passing frequency gives us a 'wavelength' typical of the structure. Figure 15 shows that this seems to increase fairly linearly with velocity.

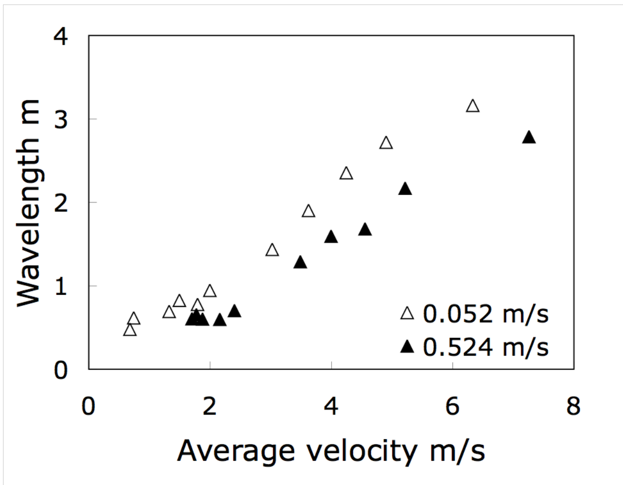

Figure 15: Structure wavelength against velocity at non-dimensional radius of 0.1875. Numbers in the legend are liquid superficial velocity in ms^{-1}.

We now consider 2 typical flow conditions, one below the transition point on the passing frequency graph, and the other well above the transition. Figure 16 shows concentration time-series for the lower point - clearly showing large scale 'bubbles' separated by liquid zones containing smaller quantities of (presumably) dispersed gas.

The 'bump' on the curve at the back of each bubble is taken to be the swelling zone described by Sekoguchi *et al* and is typical of many of the flow conditions. 3-D images in Azzopardi *et al* (Figure 14 of that paper) show the bubbles in these conditions as being irregular in shape at both nose and tail.

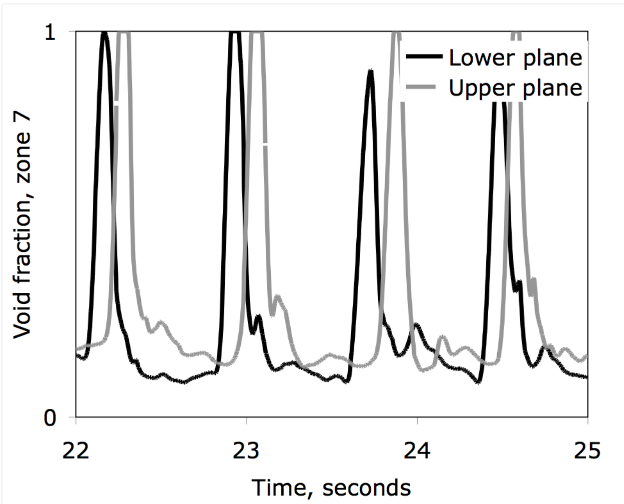

Figure 16: Example time series data for liquid superficial velocity of 0.052 ms^{-1} and gas superficial velocity of 0.077 ms^{-1}.

Considering now flows above the transition shown in Figure 17, it is clear that the flow is essentially a gas core with occasional liquid structures passing at high velocity. (The velocity is Figures 16 and 17 is of course indicated by the time delay between the time-series in each of the image planes).

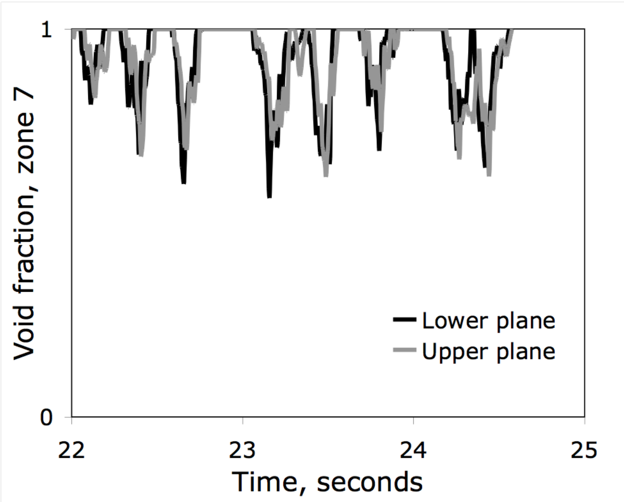

Figure 17: Example time series data for liquid superficial velocity of 0.524 ms^{-1} and gas superficial velocity of 3.446 ms^{-1}.

This wave structure is shown in cross-section in Figure 18, and we believe is entirely consistent with the pictures of huge waves shown by Sekoguchi *et al*.

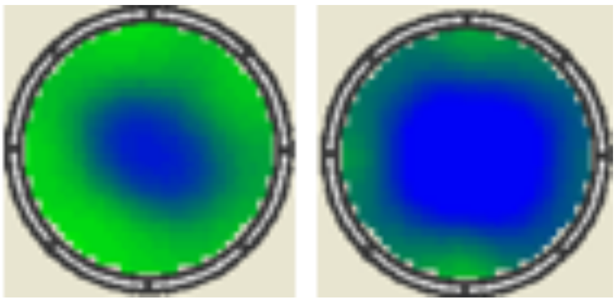

Figure 18: Example images of wave structure. Left shows wave passing through plane with zone 7 approximately 70% void, right shows the 'lull' between waves with zone 7 100% void.

Conclusions

Our results demonstrate that ECT measures flow structure velocity rather than gas velocity, where those structures are typically small bubbles, large 'churn' bubbles', and 'huge waves' as described by Sekoguchi and Mori (1997). Given the capabilities of ECT to measure velocity non-intrusively we have been able to show detailed void fraction and velocity profile information for these flows.

We observe three types of flow in these experiments: dispersed bubble, plug and huge wave. In dispersed bubble flows at higher liquid velocities and low gas flowrate the velocity profile exhibits a centre-peak, while for plug flows we a see flat velocity profile. An important transition is seen at a gas superficial velocity of about 1 ms^{-1} as huge waves become the dominant feature with a significant centre peak to the velocity profile. At this transition the velocity of the wave structure is about 2ms^{-1} and the transition is clearly measurable by the frequency of flow structures. Below the transition (in plug flow) the frequency increases with gas superficial velocity while above the transition (with huge waves dominant) the frequency is approximately constant.

Below the transition point the bubble are large, irregular 'churn' bubbles which seem to 'tunnel' up the pipe into the fast-moving wake of the bubble in front. We believe that the transition point is associated with the moment at which gas from one plug structure 'breaks through' the liquid barrier to the higher one and a continuous gas core starts to exist in the flow.

Acknowledgements

The authors would like to thank John Pendleton of Tomoflow Ltd for software support and Bill Lionheart of Manchester University for contributing to lively discussions on permittivity modelling.

References

Azzopardi B.J., Abdulkareem L.A., Zhao D., Thiele S., da Silva M.J., Beyer M. and Hunt A. Comparison Between Electrical Capacitance Tomography and Wire Mesh Sensor output for air/silicone oil flow in a vertical pipe, 3rd International Workshop on Process Tomography (IWPT-3), Tokyo, Japan (2009)

Byars M. Developments in Electrical Capacitance Tomography. Keynote review, 2nd World Congress on Industrial Process Tomography (WCIPT-2), Hannover, Germany. (2001)

Couet B., Brown P. and Hunt A. Two-phase bubbly-droplet flow through a contraction: experiments and a unified model. Int. J. Multiphase Flow Vol. 17, 291-307. (1991)

Hunt A. Deriving density information from permittivity images. Private communication with W. Lionheart (unpublished). (2007)

Hunt A., Pendleton J. and Byars M. Non-intrusive measurement of volume and mass using electrical capacitance tomography. ESDA 2004-58398, 7th Biennial ASME Conference on Engineering System Design and Analysis, Manchester, UK. (2004)

Hunt A., Pendleton J. and Ladam Y. Visualisation of two-phase gas-liquid pipe flow using electrical capacitance tomography. ESDA 2004-58396, 7th Biennial ASME Conference on Engineering System Design and Analysis, Manchester UK. (2004)

Jeffrey, D.J. Extension of the Maxwell-Wagner equation for conducting dielectrics. J. Phys. D: Appl. Phys., 9, pp L93-L95. (1976)

Nicklin D.J., Wilkes J.O. and Davidson J.F. Two-phase flow in vertical tubes. Trans. Instn. Chem. Engnrs. Vol. 40, 61-68. (1962)

Prasser H.-M., Misawa M. and Tiseanu I. Comparison between wire-mesh sensor and ultra-fast X-ray tomograph for an air-water flow in a vertical pipe. Flow Measurement and Instrumentation, Vol. 16, 73-83 (2005)

PTL Application note AN2. Calculation of volume ratio for ECT sensors, Issue 4, October 1999. Process Tomography Ltd, www.tomography.com.

Sekoguchi K. and Mori K. New development of experimental study on interfacial structure in gas-liquid two-phase flow. Experimental Heat Transfer, Fluid mechanics and Thermodynamics 1177-188. (1997)

Sillars, R.W. The properties of a dielectric containing semi-conducting particle of various shapes. J. IEE Vol. 80, 378-293. (1937)

Wagner, K.W. (1914). Erklärung der dielektrischen Nachwirkungsvorgänge auf Grund Maxwellscher Vorstellung. Arch. Elektrotech. 3, pp. 371-387.

van Beek, L. K. H. Dielectric behavior of heterogeneous systems, 69-114 in Progress in Dielectrics, Vol. 7, Edited by J. B. Birks. CRC Press. (1967)

Wagner, K.W. Erklärung der dielektrischen Nachwirkungsvorgänge auf Grund Maxwellscher Vorstellung. Arch. Elektrotech. 371-387. (1914)